Speckle Photometry and Spectral Types of Close Binary Star Components - II

Rick Wasson
Orange County Astronomers, Murrieta, California, ricksshobs@verizon.net

Abstract

Relatively few visual binary stars in the Washington Double Star Catalog have spectral types given for both components. Therefore, a speckle photometry method for observation of close binaries was developed and previously described, to simultaneously measure orbital position, derive color indices, and estimate spectral types of the individual stellar components. Eighteen additional binary stars have been observed, using the 22-inch Cassegrain reflector of the Orange County Astronomers. The method combines the techniques of speckle interferometry for diffraction-limited astrometry, Bispectrum Analysis of the relative flux distribution of the two components, and an adaptation of differential photometry for approximate photometric calibration. Observations were made in four Sloan filter bands, yielding six color indices, each of which is correlated with spectral type. The method is reviewed and astrometry, Sloan magnitudes, color indices and estimated spectral types of the individual binary components are presented and discussed.

1. Introduction

Speckle interferometry and analysis are standard techniques used by professional astronomers for about 50 years to make astrometric observations of visual binary stars, measure orbits, and determine stellar masses and ages (Davidson et al 2009). Measurement of color indices and corresponding spectral types of the individual components can provide useful supplementary information to support binary orbit solutions and more accurate definition of stellar masses and other properties for both the individual components and the total binary system (McAlister 1985, and Horch et al 2001, 2004 and 2006).

A suite of excellent free Windows-based software packages developed by David Rowe, CTO of PlaneWave Instruments, now enables amateurs and students to join in speckle interferometric observations of double stars with small telescopes. These programs make it easy to select appropriate targets from the Washington Double Star Catalog (WDS) (Rowe 2017) and the Gaia DR2 database (Rowe 2018). The Speckle Tool Box (STB) program performs Fourier Transform and autocorrelation analysis of speckle images (Rowe & Genet 2015) and (Harshaw, Rowe & Genet 2017). In 2017 Rowe completed extension of his software to the powerful technique of Bispectrum (triple correlation) analysis (Rowe 2020), employed by professional astronomers for about the last 20 years. The technique recovers the plane wave phase information distorted by the atmosphere, eliminating the 180-degree uncertainty of autocorrelation, and allowing reconstruction of a diffraction-limited image with the correct flux of each component. Correct flux enables measurement of Δmagnitude between the two stellar components.

Since 2015, the author has made speckle interferometry observations of binary stars with the 22-inch Cassegrain telescope of the Orange County Astronomers (OCA) club, located at a good site near Anza, CA (Wasson, 2018). In 2017 he began processing speckle observations with the STB Bispectrum software (Wasson, 2019).

In 2020 and early 2021, the author made the first Speckle Photometry observations with the C-11 telescope of the Fairborn Institute Remote Observatory (FIRO) (Marchetti, Caputo, and Genet, 2020). These observations were used to develop observing techniques and data reduction methods, successfully validating the capability to measure component star magnitudes and correlate the color indices to spectral type (Wasson, Genet and Rowe, 2021 and 2022). That is referred to below as paper

I. Additional 2021 observations reported here were made using the same speckle photometry technique. The correlation between color indices and spectral type – for Main Sequence stars only – was based on the tables of (Mamajek, 2019), which use classical Johnson-Cousins B V Rc Ic colors. The transformations of (Rogers et al, 2006) for the Sloan/SDSS filter set were used for correlation of spectral type with the commercially available Astrodon "Sloan generation 2" g' r' i' z' filters used here.

2. Equipment

All observations were made with the OCA 22-inch Cassegrain telescope shown in Figure 1, located about 25 km east of Mt. Palomar Observatory at an elevation of 1500 m. The camera was a ZWO ASI 6200MM cooled "full frame" CMOS (detector 24mm x 36mm). Installed in the manual focuser ahead of the camera were a 2.5X Barlow lens for f/20, and an automated ZWO 5-position filter wheel with clear and Sloan g', r', i', z' Generation 2 filters from Astrodon. The camera was controlled by SiTech ZWOCam software (Gray 2020).

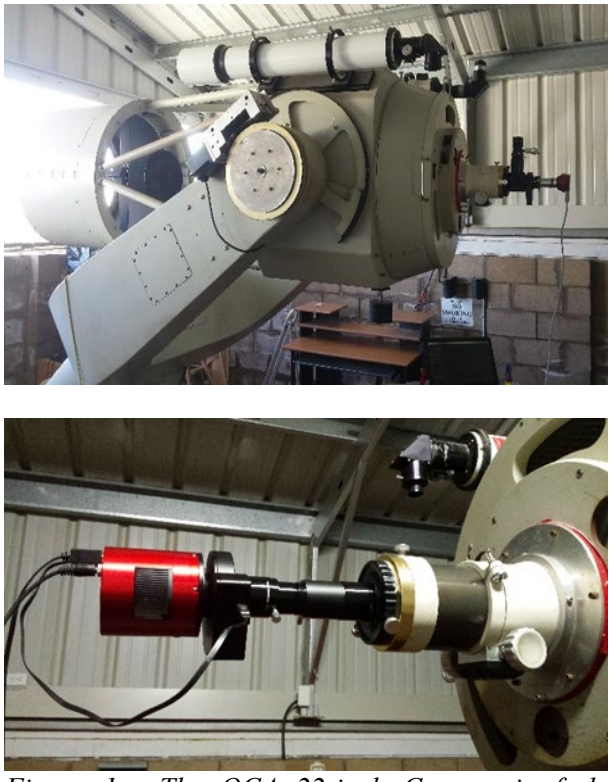

Figure 1. The OCA 22-inch Cassegrain fork-mounted telescope (above), with the speckle photometry instrumentation (below).

The Astrodon filter characteristics, shown in Table 1, were designed to match wavelengths of the Sloan Digital Sky Survey (SDSS) as closely as possible, but have higher transmission (up to 99%). Full width at half maximum transmission (FWHM) was based on manufacturer's literature. Equivalent center WL was estimated from filter transmission convolved with camera QE. To maximize sensitivity in the z' band, the Astrodon z'_2 long-pass filter was chosen, which extends throughout the camera sensitivity range, assumed to end at 1050nm.

Table 1. The Astrodon Sloan filter set used for all observations. Equivalent center WL was estimated from filter transmission convolved with camera QE, with estimated peak QE=80%. Filter FWHM is based on manufacturer's transmission literature.

Filter Characteristics Summary		
Filter	Convolved	
	Center WL (nm)	FWHM (nm)
g'	485	144
r'	624	128
i'	758	144
z'	871	178

3. Target Selection

Candidate binary systems were found in the WDS Catalog using the WDS 1.2 program (Rowe 2017) using the following search limits:

0.3" < separation < 3" primary magnitude > 6
declination > 0 Δmagnitude < 5.

The selected stars have note "O" (published orbit). From the many such WDS binaries, the online AAVSO Photometric All-Sky Survey Catalog APASS (DR10) was searched to find stars having a complete set of Sloan g' r' i' z' magnitudes (https://www.aavso.org/apass). Photometry in APASS10 is valid for 7 < V < 16, which includes all the stars observed. All but one of these binaries had the desired APASS10 Sloan data, but a few magnitudes may be based on only 1 or 2 survey

images, possibly increasing photometric uncertainty.

The characteristics of the 18 binary star systems observed are summarized in Table 2.

Table 2. Summary of characteristics of the binary stars observed by the Speckle Photometry method. The first four columns are from the WDS Catalog: WDS coordinates and Discovery code, magnitude (assumed to be V band) for primary (M1) and secondary (M2) stars, and spectral type. The next four columns are from the WDS 6th Orbit Catalog: predicted position angle (θ) and separation (ρ) on 2021.0, orbit grade, and orbital period. The last four columns are the unresolved APASS10 magnitudes in the Sloan g' r' i' z' filters.

WDS				6th Orbit Catalog (2021.0)				APASS10			
Name	M1	M2	Spectrum	θ (deg)	ρ (")	Grade	Period (yr)	g'	r'	i'	z'
01024+0504	8.49	10.07	K2+K8	53.3	0.643	2	28.2	9.371	7.731	7.402	7.327
HDS 135AB											
01166+1831	8.61	12.2	G5	221.3	0.591	5	144	8.676	8.318	8.227	7.967
HDS 169											
01388-1758	12.7	13.2	M5.5V+M6V	331.8	1.658	2	26.3	12.854	11.403	9.224	7.922
LDS 838											
17066+0039	8.73	9.81	G0	176.1	1.075	4	384	8.579	8.104	7.920	7.786
BU 823AB											
17457+1743	9.37	9.59	K0	22.7	0.678	4	600	9.025	8.256	8.133	7.931
STF2205											
17465+2743	10.2	10.7	M3.5V	21.3	0.864	1	43.1	-	-	-	-
AC 7BC								*Used Gaia(DR2) + ATLAS*			
17506+0714	8.18	8.98	F2	162.9	0.611	4	1000	7.933	7.586	7.487	7.551
STT 337											
18320+0647	7.84	8.91	F5V	217.6	0.563	4	426	7.783	7.324	7.237	7.381
STT 354											
19019+1910	8.41	8.83	G5	1.3	0.557	4	805	8.074	7.765	7.765	7.466
STF 2437											
20290+0710	9.52	9.91	G0	97.9	0.459	3	171	9.076	8.679	8.629	8.417
A 610											
20329+1142	10.04	10.57	?	55.8	2.128	5	528	10.095	9.173	8.963	8.790
J 1AB											
20329+1357	10.6	10.92	K0	133.7	0.496	2	118	10.389	9.535	9.286	9.167
L 35CD											
20524+2008	7.98	8.95	F5+A0	347.2	0.361	4	1644	7.865	7.479	7.400	7.040
HO 144											
21186+1134	7.31	8.88	G0V+G6V	77.0	0.939	2	78.5	7.540	6.575	6.498	6.568
BU 163AB											
22419+2126	8.64	9.55	G0	51.6	1.519	4	1210	8.507	8.037	7.859	7.987
STF 2934											
22557+1547	9.23	9.73	G5	74.1	1.215	3	213	8.696	8.491	8.349	8.116
HU 987											
23024+1837	9.58	10.04	G5	296.3	0.489	3	153	9.130	8.548	8.401	8.684
HU 398											
23409+2022	8.50	10.81	K2	185.4	1.020	5	125	8.779	7.476	7.036	7.082
HO 303AB											

4. Observing Procedure

The speckle photometry observation procedure consists of repeated "Sets" of exposures. Within each set, for one filter, 7 long (~1-5 sec) exposures

are taken, followed by ~500 short (<0.1 sec) speckle exposures, followed by another 7 long exposures, all in the same camera Region of Interest (ROI). The next filter is immediately cycled into position, and the exposure sequence is repeated. Completion of all the exposures for all four filters constitutes a complete set. One set is summarized as:

g′: 7 Long	500 Speckle	7 Long
r': 7 Long	500 Speckle	7 Long
i': 7 Long	500 Speckle	7 Long
z': 7 long	500 Speckle	7 Long

Within each set the filters are cycled as fast as possible because they are later used to create color indices for that set. The speckle exposures are bracketed by long exposures, which are later stacked to produce one image with high signal/noise ratio (SNR) that bridges the speckle exposures in time and experiences approximately the same atmospheric conditions. This is an attempt to account for photometric variations caused by atmospheric extinction, similar in some ways to capturing Variable and "Comparison" stars simultaneously in conventional CCD photometry.

Typically, four independent sets are taken, for the purpose of evaluating photometric variations. A fifth set of speckle-only exposures of a single Reference Star is made in the middle of the series of sets. These Reference Star exposures are not used in any photometric way; they are used later in standard speckle deconvolution processing to remove optical aberrations that appear in both the binary and single star images.

5. Astrometry Results

The speckle Bispectrum astrometry results are summarized in Table 3, where average and standard deviation of position angle and separation for all sets and filters are highlighted in yellow. Bispectrum Analysis yields a reconstructed, diffraction-limited image of the binary star, from which the astrometric measurements of separation and position angle are made. All speckle frames were analyzed using the Bispectrum "tools" in the STB software (Rowe 2020).

Calibration of image scale (arc-sec/pixel) and camera orientation on the sky was done by plate solving several full-frame images of the area surrounding the target star on each night. PlateSolve 3.78 software (Rowe, 2021) uses the UCAC4 stellar database, producing remarkably uniform solutions, and more accurate calibration than any other method known to the author. Even though the field of the large format camera was small at f/20 (10.9'x7.3' for 11-meter focal length), 5-second exposures in the clear filter gave enough stars for successful solutions in all cases when approximate coordinates were provided to the program.

The astrometric uncertainties in Table 3 benefited from measurements in four filters, repeated in several sets. Also included are Δmagnitude results, but these were not used directly for estimation of spectral types (see Section 7). Unsuccessful or poor-quality observations, generally caused by a very faint combination of secondary star color and filter, are noted in orange.

6. Flux Proportions

Two photometric factors are of paramount importance in this Speckle Photometry method:

1. The proportion of flux attributed to each component of the binary. These Flux Proportions are products of Bispectrum Analysis.
2. The overall calibration of the combined (unresolved) light of both components to the standard Sloan/SDSS photometric system. Photometric calibration is derived from the "long" seeing-limited exposures, discussed in Section 7.

Bispectrum Analysis, also known as triple correlation, was performed on the speckle frames, utilizing the Reference Star images for deconvolution. The wave front entering the telescope is ideally like a flat sheet of paper – a plane wave front. But the atmosphere distorts, disperses, advances, and delays all parts of the wavefront in random ways, as though the smooth paper had been tightly crumpled and then unfolded again. The irregular sheet is something like the phase distortion of the original plane wave front, redirecting the light in many divergent ways.

For all 500 speckle frames Bispectrum Analysis examines and correlates the light deviations of all the pixels – an intense number-crunching process. From these correlations the distortions in all the

images are repaired, recreating the average image that would have come from a nearly undistorted plane wavefront – as though the crumpled paper had been pressed flat again. The end product of Bispectrum Analysis is a single reconstructed, phase-corrected, diffraction-limited image.

Typical examples of Bispectrum images are shown in Figure 2 for HDS135AB, the first binary star in Tables 2 and 3.

Table 3. Summary of astrometric measurements. The columns are: Target (WDS coordinates and discovery designation), Date (calendar and Besselian), Sloan filter, number of sets observed. The following columns give the average of the sets for position angle (θ), standard deviation of θ, separation (ρ), standard deviation of ρ, Δmagnitude and standard deviation of Δmagnitude. For θ and ρ, the statistics are for the number of sets in each filter. Overall average and standard deviation of ρ and θ, for all filters and sets, are shown in yellow.

Target	Date	Filter	# Sets	θ (deg)	σ(θ)	ρ (")	σ(ρ)	Δmag	σ(Δmag)
01024+0504	2021-10-28	g'	4	55.08	0.81	0.648	0.008	2.548	0.086
HDS 135AB	2021.824	r	4	54.27	0.40	0.652	0.005	1.953	0.033
		i'	4	54.78	0.25	0.656	0.004	1.653	0.030
		z'	4	54.70	0.42	0.647	0.014	1.500	0.104
				54.71	0.55	0.651	0.009		
01166+1831	2021-11-03	g'	1	216.91	-	0.588	-	6.170	-
HDS 169	2021.841	r	3	219.13	0.64	0.602	0.029	4.827	0.218
		i'	3	218.28	0.88	0.530	0.016	3.377	0.181
		z'	4	217.12	2.59	0.589	0.048	3.675	0.910
				217.96	1.76	0.576	0.043		
01388-1758	2021-11-03	g'	-						
LDS 838	2021.841	r	4	332.65	1.02	1.661	0.050	2.313	0.352
		i'	4	333.20	0.14	1.669	0.010	0.600	0.022
		z'	4	333.48	0.27	1.723	0.097	0.550	0.083
				333.11	0.66	1.684	0.064		
17066+0039	2021-08-12	g'	4	177.69	0.40	1.060	0.008	1.700	0.149
BU 823	2021.613	r	4	177.31	0.12	1.059	0.008	1.203	0.098
		i'	4	177.12	0.17	1.056	0.003	1.038	0.026
		z'	4	176.89	0.40	1.054	0.008	0.890	0.051
				177.25	0.41	1.057	0.007		
17457+1743	2021-08-16	g'	4	19.92	0.30	0.796	0.002	0.275	0.093
STF2205	2021.624	r	4	20.14	0.19	0.798	0.001	0.285	0.024
		i'	4	19.93	0.12	0.798	0.003	0.235	0.065
		z'	4	20.71	0.40	0.793	0.008	0.180	0.134
				20.17	0.41	0.796	0.005		
17465+2743	2021-09-07	g'	4	26.06	3.99	0.934	0.040	1.438	0.883
AC 7BC	2021.684	r	4	26.76	0.35	0.961	0.008	0.725	0.139
		i'	4	26.92	0.20	0.963	0.004	0.573	0.030
		z'	4	26.00	0.45	0.956	0.009	0.540	0.047
				26.56	0.53	0.960	0.007		
17506+0714	2021-09-12	g'	4	162.88	0.14	162.883	0.001	0.333	0.034
STT 337	2021.698	r	4	163.12	0.43	0.619	0.008	0.265	0.026
		i'	4	163.29	0.29	0.615	0.008	0.280	0.061
		z'	4	163.33	0.58	0.608	0.002	0.293	0.100
				163.15	0.40	0.616	0.008		
18320+0647	2021-09-03	g'	4	204.88	0.14	0.501	0.004	1.283	0.043
STT 354	2021.674	r	4	204.29	0.76	0.495	0.002	1.093	0.053
		i'	4	203.07	0.49	0.500	0.001	1.203	0.090
		z'	4	204.18	0.41	0.519	0.006	1.263	0.102
				204.10	0.81	0.504	0.010		
19019+1910	2021-10-10	g'	3	332.51	0.11	0.568	0.002	0.527	0.035
STF 2437	2021.775	r	3	332.27	0.20	0.567	0.003	0.490	0.040
		i'	3	332.39	0.09	0.566	0.004	0.580	0.080
		z'	3	334.22	1.19	0.571	0.005	0.607	0.199
				332.85	0.98	0.568	0.003		

Table 3. Continued.

Target	Date	Filter	# Sets	θ (deg)	σ(θ)	ρ (")	σ(ρ)	Δmag	σ(Δmag)
20290+0710	2021-08-16	g'	4	98.01	0.26	0.520	0.005	0.560	0.028
A 610	2021.624	r	4	98.31	0.32	0.510	0.004	0.460	0.053
		i'	4	97.99	0.48	0.531	0.005	0.493	0.142
		z'	4	99.06	1.55	0.555	0.011	0.600	0.311
				98.34	0.87	0.529	0.018		
20329+1142	2021-09-12	g'	2	62.81	0.14	2.116	0.004	1.005	0.021
J 1AB	2021.698	r	2	62.78	0.04	2.113	0.003	0.780	0.010
		i'	2	62.74	0.06	2.111	0.001	0.620	0.010
		z'	2	62.91	0.16	2.109	0.008	0.545	0.078
				62.81	0.11	2.112	0.004		
20329+1357	2021-08-12	g'	4	128.38	2.16	0.500	0.033	0.340	0.208
L 35CD	2021.613	r	4	129.91	0.98	0.521	0.005	0.493	0.022
		i'	4	129.17	1.35	0.520	0.009	0.585	0.164
		z'	4	129.60	2.58	0.523	0.020	0.688	0.457
				129.26	1.78	0.516	0.020		
20524+2008	2021-09-07	g'	4	348.31	0.45	0.432	0.001	0.325	0.066
HO 144	2021.684	r	4	348.48	0.70	0.431	0.004	1.015	0.066
		i'	4	347.44	2.36	0.432	0.008	1.640	0.088
		z'	4	350.10	1.54	0.439	0.021	1.570	0.149
				348.58	1.65	0.434	0.011		
21186+1134	2021-09-07	g'	4	76.94	0.38	0.961	0.010	1.850	0.022
BU 163AB	2021.684	r	4	77.36	0.32	0.954	0.004	1.678	0.034
		i'	4	76.54	0.17	0.964	0.004	1.728	0.032
		z'	4	76.67	0.52	0.963	0.005	1.643	0.061
				76.88	0.46	0.961	0.007		
22419+2126	2021-10-10	g'	4	55.04	0.09	1.402	0.002	1.168	0.062
STF 2934	2021.775	r	4	55.05	0.07	1.407	0.001	0.995	0.045
		i'	4	55.07	0.06	1.405	0.004	0.915	0.006
		z'	4	55.05	0.19	1.406	0.007	0.945	0.019
				55.05	0.11	1.405	0.004		
22557+1547	2021-10-28	g'	4	74.56	0.27	1.252	0.004	0.838	0.074
HU 987	2021.824	r	4	74.46	0.05	1.254	0.005	0.690	0.012
		i'	4	74.39	0.09	1.251	0.003	0.648	0.013
		z'	4	75.23	0.88	1.226	0.025	0.563	0.130
				74.66	0.54	1.246	0.016		
23024+1837	2021-10-28	g'	4	298.66	0.50	0.495	0.003	0.593	0.062
HU 398	2021.824	r	4	299.08	0.51	0.494	0.004	0.618	0.068
		i'	4	298.95	0.50	0.501	0.003	0.658	0.038
		z'	3	300.22	2.12	0.484	0.006	0.520	0.139
				298.90	0.49	0.497	0.004		
23409+2022	2021-11-03	g'	4	185.36	0.26	0.956	0.005	2.478	0.088
HO 303AB	2021.841	r	4	185.81	0.17	0.968	0.003	2.093	0.046
		i'	4	186.18	0.26	0.962	0.003	1.540	0.029
		z'	4	186.61	0.27	0.959	0.002	1.420	0.026
				185.99	0.52	0.961	0.006		

The Δmagnitude uncertainties in Table 3 are often reasonably good [i.e., σ(Δmag) <0.05]; but sometimes they are quite poor when the secondary star is faint. The r' and i' filters usually give the best results, while g' and z' are often worse. These variations are generally related to the brightness and

color of the individual stars, and to camera quantum efficiency (QE). That is, photometric accuracy is probably driven by SNR of the two stars in the Bispectrum image.

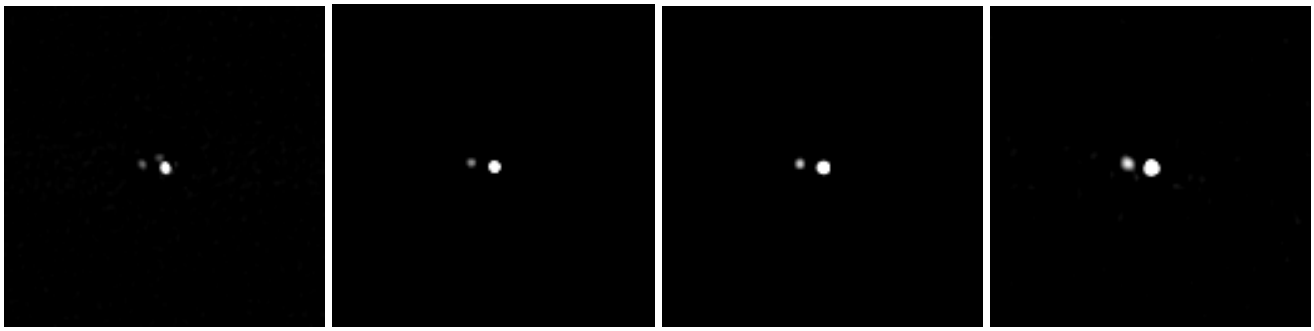

Figure 2. Reconstructed diffraction-limited images of 01024+0504 HDS135AB, with North up, East left. The images are 128x128 pixels (9"x9") in size and component separation ρ=0.65". Left to right: Sloan g' r' i' z' filters. The V~10 secondary of this K2+K8 pair is relatively faint in g' and even in r', but brighter in i' and z' because it is red, and better seeing allows longer speckle exposures to compensate for lower camera QE.

Since the Bispectrum image approaches zero wavefront error, it contains approximately the correct flux for each component star. In the STB program, measurement tools use three circular apertures to measure the ADU flux of the two stars and the background level. The background aperture is located away from the stars, rather than in an anulus centered on a star, typically of wider-field photometry for single or unresolved stars. The same Bispectrum image and apertures are used to simultaneously measure the net flux for photometry and the centroid of the net flux for astrometry.

Slightly different aperture sizes would have little effect on centroids for astrometry. However, for photometry the *same size aperture* must be used for both stars, to measure the same *proportion* of total light for them. This is because both stars have the same point spread function (psf); the primary appears larger only because its psf arises higher above the background.

The apparent brightness of each binary component is measured as the Flux Proportion (FP), defined in equation (1), where A and B indicate the primary and secondary stars, respectively, and ADU is the net signal within an aperture. By definition, the sum of the A and B Flux Proportions is always 1.0.

$$FP_A = ADU_A / (ADU_A + ADU_B)$$
$$FP_B = ADU_B / (ADU_A + ADU_B) \quad (1)$$

Examples of Flux Proportions for two binary stars are shown in Figure 3 to illustrate their repeatability. The blue symbols and line represent the primary (A) star, while red indicates the secondary (B) star. The two stars are one of the *best* cases (01024+0504 HDS135AB) and one of the *worst* cases (20329+1357 L35CD) of Δmagnitude uncertainty from Table 3. For each binary, all four sets of filter measurements are plotted for both component stars; many points overlap, showing good repeatability.

The factor that probably plays a major role in repeatability of Flux Proportions is SNR. For HDS135AB, the primary star had consistently high SNR, between 100 and 200 for all sets of filters, while the SNR of the secondary star ranged from only 5 to 68. For simplicity, SNR is taken to be (net ADU) / (Background ADU) within the STB aperture, although the background may not include all the noise sources. Since the Flux Proportions of both stars are intimately linked together in equation (1), they are both good, even though Δmag >1.5 and the secondary component has low SNR.

This unexpected result indicates that high SNR of the bright star dominates the result, apparently minimizing the uncertainty of both Flux Proportions, at least for high Δmag pairs. This effect is supported by the opposite result for 20329+1357 L35CD, which has low SNR and poor repeatability because *both stars are faint*, even though Δmag is only ~0.3. As seen in Figure 3, the greatest uncertainties occurred in the g' and z' bands. The *primary* SNR values were: (15<SNR<18) for g' and (20>SNR<26) for z', respectively. The r' results

are much better, apparently because SNR is higher (63<SNR<104).

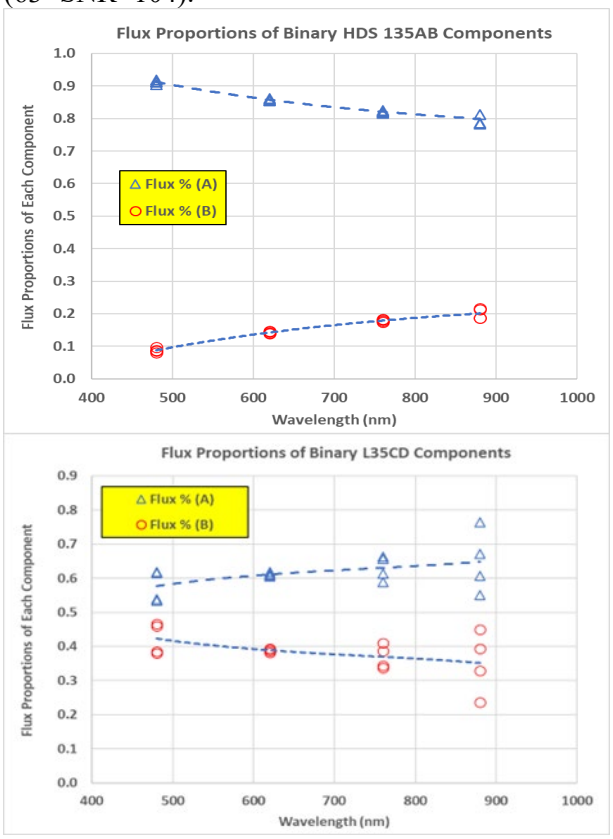

Figure 3. Above: Binary star 01024+0504 HDS135AB, an example of good repeatability of Bispectrum Flux Proportion. The WDS magnitudes are V=8.49/10.07. The groups of four points are centered at the g′ r′ i′ z′ center wavelengths, respectively (Table 1). Below: Binary star 20329+1357 L35CD, an example of poor repeatability of Bispectrum Flux Proportions. WDS magnitudes are V=10.04/10.57, but the overall spectral type of this binary is not given in WDS.

A second factor which probably degrades repeatability of Flux Proportions is variable atmospheric extinction, which can change both apparent brightness (SNR) and color. Bracketing each series of speckle images between two groups of "long" exposures (Section 7) is a strategy intended to minimize the effects of variable extinction. Observations were made only on clear nights with no sign of clouds or haze, but thin unnoticed clouds could still cause scattered photometric data.

7. Photometry Calibration

Deep CCD exposures taken in large surveys such as SDSS, Pan-STARRS, and APASS, provide a source of magnitudes of the *unresolved* binary star transformed to the standard Sloan photometric system. The "long" exposures in the speckle photometry method utilize the same filter and camera small ROI as the speckle exposures. During the "long" exposures, typically 1-5 seconds, the atmosphere mixes the close binary components into an *unresolved* seeing disk, just as it does in the survey images. Figure 4 shows an example of Bispectrum and long exposure images at the same scale.

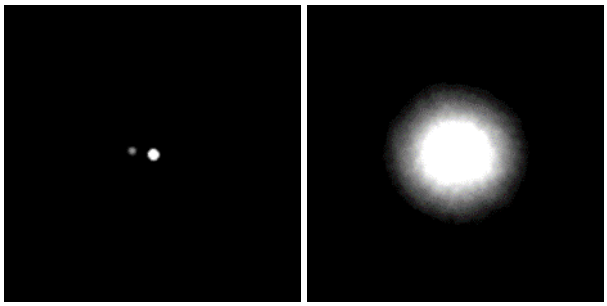

Figure 4. 01024+0504 HDS135AB images in the r′ filter. Left: a diffraction limited Bispectrum image, separation ρ=0.65" after processing 500 20-msec images. Right: a stack of 14 long (1-sec) unresolved exposures, 7 taken immediately before and 7 following the speckle exposures. Both images are 128x128 pixels, 9"x9" in size.

This approach of taking long exposures of the binary star itself is a sort of variation on the common practice of differential photometry of variable stars. But the high-magnification requirement of speckle limits the field of view severely, making simultaneous comparison and check stars inaccessible. Relying on survey Sloan magnitudes, the target binary itself plays the role of a "secondary standard" comparison star, providing approximate self-calibration to transform the instrumental magnitude to the standard photometric system, and avoiding the separate comparison, extinction, and transformation stars of conventional photometry

The compromise in this method, of course, is that the binary star is *not a "photometric standard" star,* so its magnitudes on the Sloan system are much less accurate than true standard stars, and it may even be variable. However, the goal of the speckle photometry method is not to produce accurate

photometry for light curve comparisons with other observers, such as is needed for variable stars. The goal here is only to produce *self-consistent* magnitudes among the four filters, within one set, in order to provide *color indices* on the standard Sloan system that correlate with *spectral types* of the *resolved* binary component stars.

The long images are stacked to produce a single image with high SNR and a more symmetric psf, also averaging small extinction variations. The flux is measured in STB with a photometric aperture larger than the seeing disks, and much larger than for the two resolved stars in the Bispectrum image. The same aperture – large enough to include all the light in all four bands – is necessary for consistent color indices. If the aperture is too small, a different percentage of light may be measured for each filter, seriously impacting the color index results. For example, a 3% error in one filter will cause an error of 0.03 in color index Δmagnitude.

The net ADU flux within the aperture is converted to photoelectrons per second, to account for camera gain and different exposure times for different filters. The instrumental magnitude of the unresolved binary (A+B) is then calculated with equation (2).

$$m_{(A+B)} = -2.5 * \text{Log}_{10}(\text{Net Flux}_{A+B}) \qquad (2)$$

For each filter, the instrumental magnitude $m_{(A+B)}$ is then compared with the standard magnitude $M_{Standard}$ from survey catalogs. In practice. the AAVSO APASS photometric survey catalog, Data Release 10 (AAVSO, 2020), has generally been used. It has brighter magnitude limits, includes magnitudes for all four Sloan filters more consistently, and is more easily accessed than the surveys from large telescopes, which tend to saturate the relatively bright stars accessible by speckle with small telescopes.

A Calibration Factor for each filter is defined simply as the magnitude difference between the standard and instrumental magnitudes, equation (3).

$$Z_{A+B} = (M_{Standard} - m_{Instrumental})_{A+B} \qquad (3)$$

This calibration factor includes instrumental transformation to the standard photometric system, so it applies to only one filter at a time. It also accounts for the atmospheric extinction terms which impact photometry: air mass, sky transparency and extinction effect on color. However, the 2nd-order extinction may not be fully corrected, as discussed in Section 9.

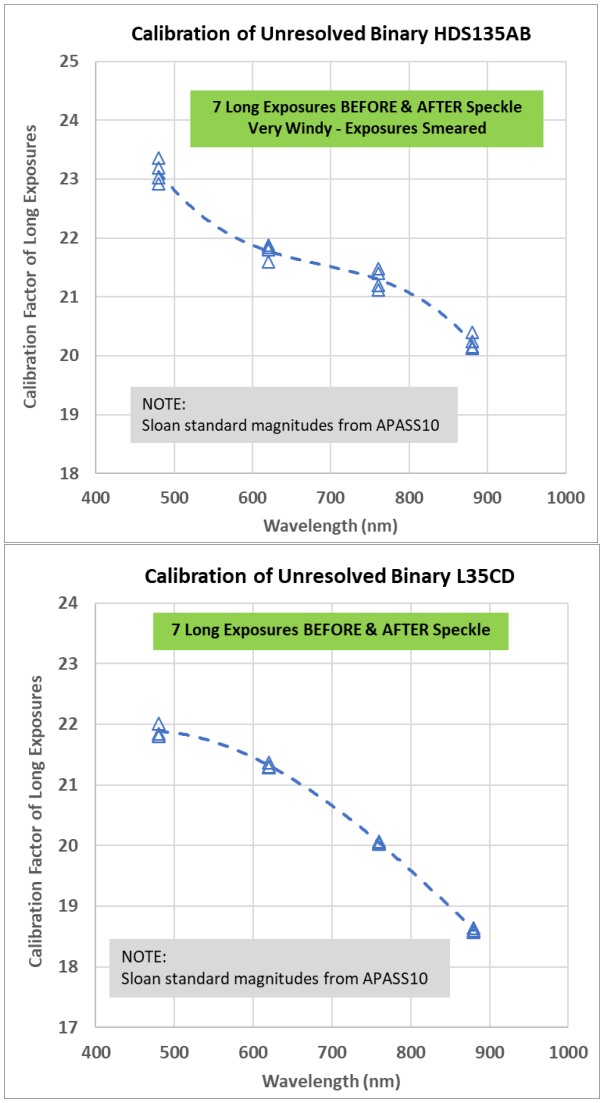

Figure 5. Calibration Factors measured for the unresolved long exposures of 01024+0504 HDS135AB (above) and 20329+1357 L35CD (below). These factors are magnitude differences calculated from equation (3). Although in Figure 3 the speckle Flux Proportions of HDS135AB have less scatter than those of L35CD, the opposite trend is seen here, possibly caused by windy conditions smearing the long images of HDS135AB.

A new series of long exposures is observed to "re-calibrate" every series of speckle frames. The calibration factors for each of the filters, $Z_{g'}$ $Z_{r'}$ $Z_{i'}$ $Z_{z'}$ respectively, are the final product of each independent set of long exposures; examples are shown in Figure 5.

A key assumption of this method is that the calibration factor, measured from the *unresolved combined* light of both components, can be applied to the *individual* A and B stellar components. This assumption seems reasonable for similar stellar types and colors, but it might cause systematic errors in the secondary star for high delta magnitude binaries, where the primary star dominates the long exposures, but A and B have much different colors or SNR.

Standard photometric image calibration using bias, dark, and flat frames was not done; therefore, some noise is present which might be suppressed by careful calibration. However, lack of calibration is mitigated by the following factors:

1. The speckle and "long" calibration frames are relatively short (a few seconds).
2. The cooled camera has very low dark current (<<1e^-/sec/pixel).
3. CMOS cameras now have very low read noise (~1.5e^-), remarkably uniform "bias" levels, and no "amp glow."
4. The highly magnified image is spread across many pixels (typically 6-8 pixels across the Airy disk) rather than only a few pixels in wide-field photometry.
5. Although no flat calibration was done, pixel variations are further averaged by random signal sampling across many pixels within the ROI due to atmospheric scattering and small tracking errors during many speckle frames and multiple "long" exposures.

Additionally, it is difficult to be certain that the small ROI used in data frames is registered to the correct pixels in full size calibration frames. Therefore, shot noise during short speckle exposures, especially for faint secondary components, is likely the dominant noise source.

8. Component Standard Magnitudes

In each filter, the instrumental net fluxes of the binary A and B components are calculated from equation (4), where the combined instrumental flux measured from the stacked long exposures [equation (2)], is simply multiplied by the respective flux proportion of each component [equation (1)] which was measured from the Bispectrum image.

$$\text{Net Flux}_A = \text{Net Flux}_{A+B} * FP_A$$
$$\text{Net Flux}_B = \text{Net Flux}_{A+B} * FP_B \quad (4)$$

The instrumental magnitude of each component is then calculated from equation (5).

$$m_A = -2.5 * \text{Log}_{10}(\text{Net Flux}_A)$$
$$m_B = -2.5 * \text{Log}_{10}(\text{Net Flux}_B) \quad (5)$$

Finally, standard magnitudes of the components are *approximated* simply by adding the calibration factor back to their instrumental magnitudes in equation (6).

$$M_{A\ \text{Standard}} \sim m_{A\ \text{Instrumental}} + Z_{A+B}$$
$$M_{B\ \text{Standard}} \sim m_{B\ \text{Instrumental}} + Z_{A+B} \quad (6)$$

This key assumption of the method bears restating: although the calibration factor is *derived from the unresolved star*, it is *applied to each component* of the binary separately, to estimate its standard magnitude. The resulting estimated standard magnitudes of the two example binary stars are shown in Figure 6.

APASS10 standard magnitudes of the unresolved binary were generally used as the "truth model" for long exposure calibration. However, APASS10 data were not available for one binary, 17465+2743 AC7BC, and sometimes there is only one exposure on which the APASS photometry for a filter is based.

Gaia(DR2) generally provides high-quality G Bp Rp photometry, unresolved or for both components. Therefore, the combined magnitudes of the A and B components from the ATLAS "RefCat2" Catalog were used for calibration of AC7BC and could be used for almost any other binary. Although an additional transformation from Gaia to the Sloan system was required, it is provided in the ATLAS RefCat2 All-Sky Stellar Reference Catalog (Tonry et al. 2018) and (Carrasco 2015). ATLAS RefCat2 is a major product of Gaia DR2; it contains photometric transformations from Gaia to other major photometric systems including the PanSTARRS version of the Sloan g' r' i' z' bands, and it provides an excellent "backup" photometry source.

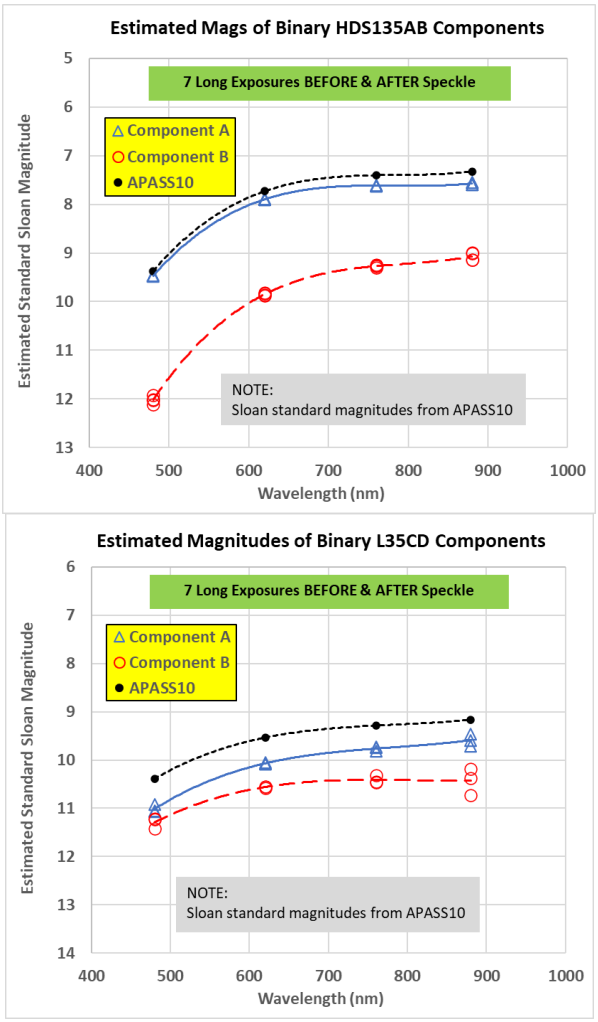

Figure 6. Estimated standard g' r' i' z' magnitudes of the resolved primary (A) and secondary (B) components, compared with unresolved APASS10. Blue symbols indicate A, red B, and black APASS10. 01024+0504 HDS135AB is above, 20329+1357 L35CD below.

9. Component Color Indices

Color index is the difference in magnitude between any two filters. The *major goal* of this speckle photometry method is to measure color indices of the A and B components of binary stars on the standard Sloan photometric system. Therefore, the four filters are observed close together in time within a set, to minimize possible effects of variable extinction. For each filter, the short speckle exposures are sandwiched between two small groups of calibration exposures. The goal of cycling filters quickly within each set is to get the most accurate possible color indices.

Six color indices are formed from the four g' r' i' z' filters: (g'-r'), (g'-i'), (g'-z'), (r'-i'), (r'-z'), and (i'-z'). Color indices are taken only from measurements within the same set. All six color indices are equally valid, but an error in any one standard magnitude will propagate into all three related color indices. Each observed set provides an independent sample of all six color indices and the overall average and statistics are derived from all the sets in a nightly observation.

Most photometric correction terms will tend to cancel in this method, as they do in differential photometry, where the variable and comparison stars are observed under nearly the same conditions. However, the 2nd-order extinction term does not cancel for stars of significantly different colors. It is not well accounted for because it contains the color index times airmass; color index is large for red stars, and airmass is never less than 1. This is analogous to using a comparison star of much different color in differential photometry. Therefore, 2nd-order extinction may add a systematic error to the magnitudes and color indices, especially for blue-red binaries.

Figure 7 shows Color Index results for the example stars, plotted with "normalized wavelength" (ΔWL / Average WL). This parameter accounts for both WL difference and the region in which the difference occurs. The normalized WL effectively places the color indices in order of *increasing sensitivity to star color*. This trend should be monotonic, although it may not be linear; nevertheless, the data are shown with simple linear regression fits for reference. APASS10 data was available for 17 of the binaries observed, and the low-high pattern seen in the g'-r' and r'-z' color indices in Figure 7 was present in all cases except for one. Of course, the speckle photometry results followed this "truth model" pattern, which may be an astrophysical or filter characteristic.

For stars on the Main Sequence, the linear regression slope should increase as spectral type gets later (redder) because all color indices get larger. This is true for the components of HDS135AB, consistent with their WDS magnitudes

and known spectral types given in Table 2, even though the APASS10 Sloan g' magnitude has a very large uncertainty.

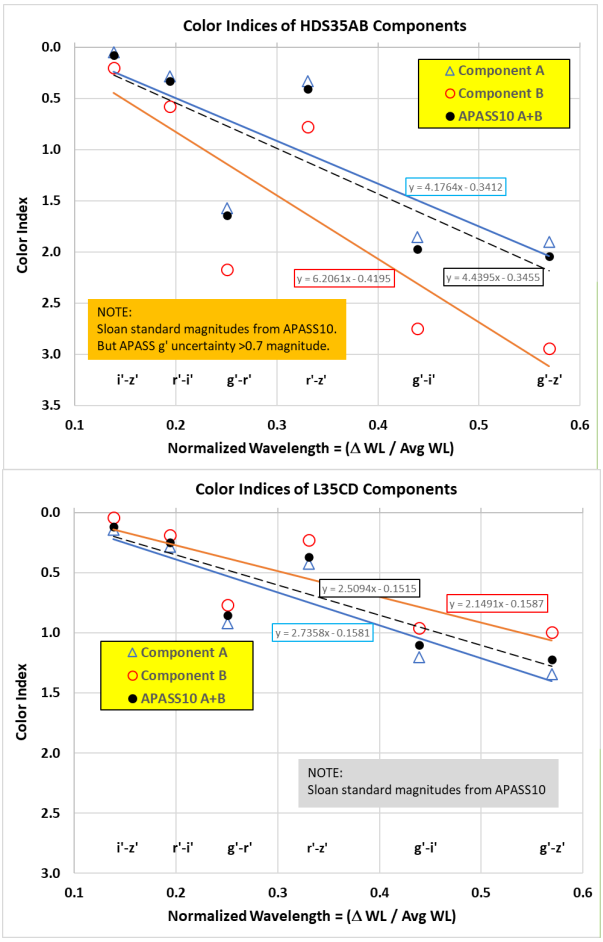

Figure 7. Color indices plotted against normalized wavelength for 01024+0504 HDS135AB (above) and 20329+1357 L35CD (below). Each point is the average of all four sets observed. The filters composing each color index are noted below the plotted points.

The trend is reversed, however, for L35CD, where the primary star (blue symbols and line) is *below* the secondary (red) and has a *steeper* slope. This may mean that the primary star – brighter, but also redder – may be a sub-giant, growing in size but cooling as it begins to leave the main sequence. There is considerable scatter in the color indices of each set, but the *average* of all six color indices, which is plotted in Figure 7, is consistently larger (redder) for the primary star than for the secondary.

Uncertainty (standard deviation) of the color indices from the four sets of observations are shown in Figure 8 for both binary components. It is clear that the uncertainties of the secondary stars are significantly greater than those of the primaries. The overall average of these color index uncertainties is 0.041 magnitude for the primary star and 0.100 magnitude for the secondary star, comparable with uncertainties estimated by Horch et al. (2001 & 2004) for small telescopes: ~0.15 magnitude.

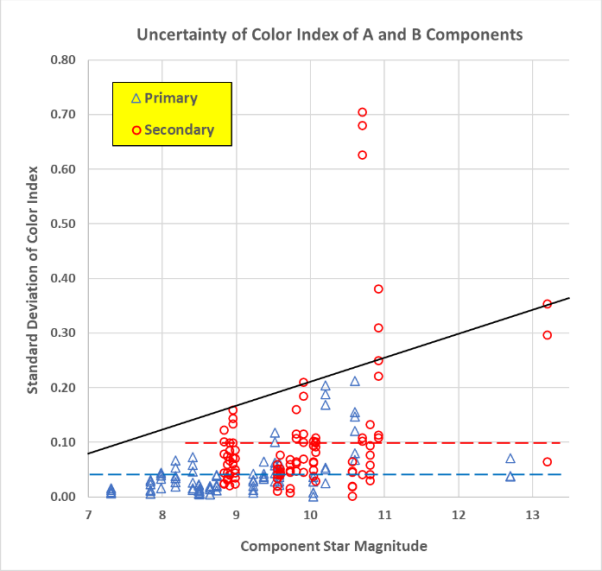

Figure 8. Uncertainties of the four sets of Color Indices for all individual components of the binaries observed. Average uncertainties for the primary and secondary stars are blue and red dashed lines, respectively.

The solid black line in Figure 8 approximates an obvious trend of increasing uncertainty with magnitude, likely caused by decreasing SNR for the limited speckle exposure time required to freeze the seeing. The highest 3 points all arise from the g' filter for the faint (V=10.7) late type (WDS M3.5V) secondary of AC7BC, which was barely detectable in g'. The four points at V=10.92 are from the g' and r' filters for L35CD, WDS spectral type K0. The 2 high points at V=13.2 involve the r' filter; this extremely faint red dwarf secondary star, WDS spectral type M6V, was not detectable at all in the g' filter. SNR could be improved by taking a larger number of speckle frames (n) for faint red targets in the short WL filters [i.e., SNR ~ SQRT(n)].

10. Component Spectral Types

The foundation of spectrophotometry was laid by correlating Johnson U B V photometry color indices with Morgan-Keenan spectroscopic standard stars (Johnson & Morgan, 1953). As detectors became more red-sensitive, the correlation was extended to the Johnson-Kron-Cousins U B V Rc Ic bands. These J-C color index relationships to spectral type were refined to a continuous set by (Pecaut & Mamajek, 2013). Further refinements for main sequence stars are maintained and updated by Mamajek, accessible on his University of Rochester web site (Mamajek, 2019) which was the source for this work. The photometric transformation of (Rogers et al, 2006) was used to adapt B V Rc Ic color indices in the Mamajek tables to the standard Sloan g' r' i' z' system.

The resulting spectrophotometric tables of Mamajek, transformed to Sloan color indices, are plotted in Figure 9. Each of the six color indices has a unique and equally valid relationship with spectral type. All the color index correlations are continuous and monotonically increase with spectral type. The Mamajek tables are limited to normal dwarf stars on the main sequence that are near enough to the Sun not to be significantly reddened by interstellar dust.

Each spectral type (letter) in the Mamajek tables is uniformly divided into a sequence of 10 sub-types from B0 through M9. A numerical integer "spectral index," corresponding to each spectral sub-type, is shown on the bottom axis of Figure 9. For an observed color index, the spectral index is used in linear interpolation to find a spectral sub-type with an added decimal point. Referring to Figure 9 for example, if the measured g'-i' color index is 1.05, then the interpolated spectral index is 43.1, giving spectral type K3.1V. In this way, each measured color index directly yields an estimated spectral type.

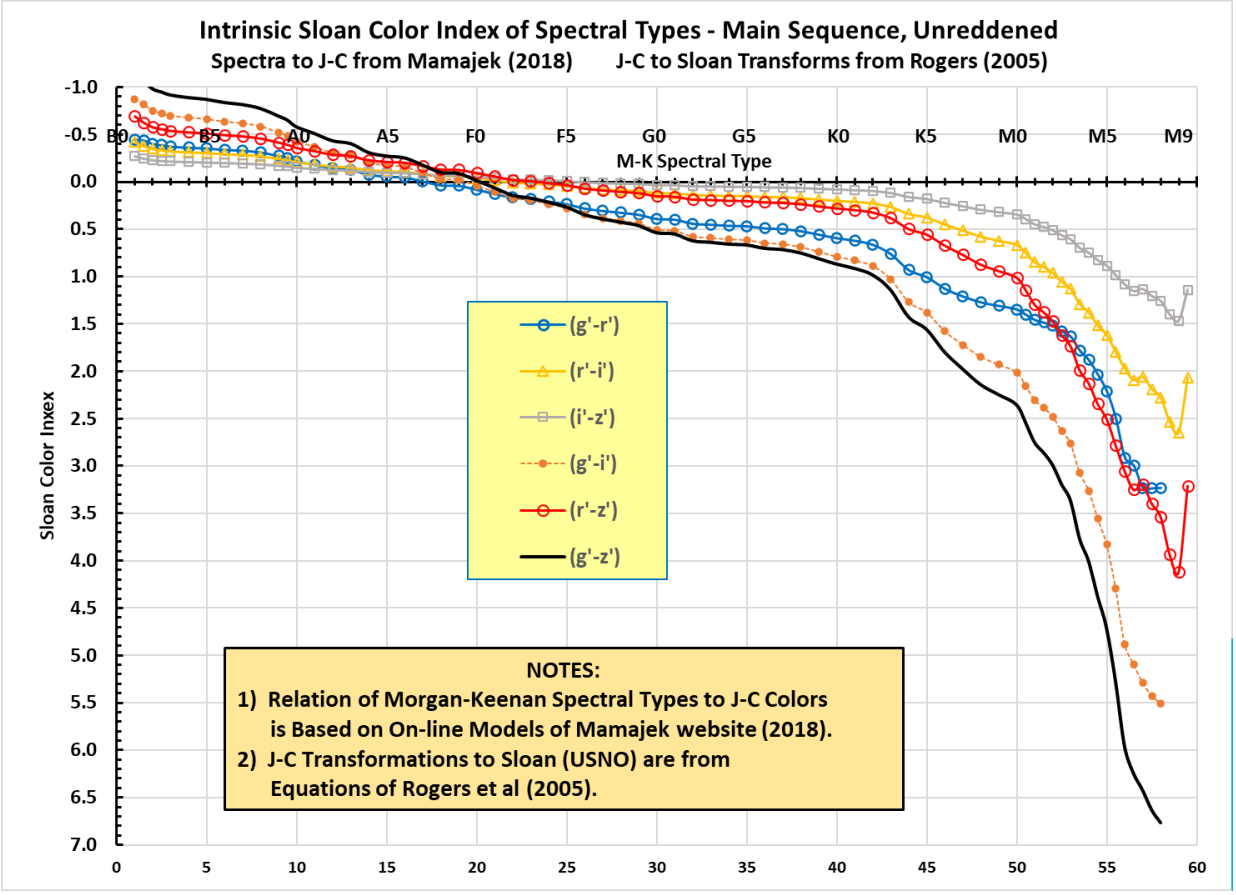

Figure 9. The relationship of Sloan filter color indices to spectral type for main sequence dwarf stars, based on the tables of Mamajek, with transformation from J-C to Sloan. Spectral type is indicated at top and the integers at bottom correspond to spectral sub-types (e.g., 30=G0, 31=G1, 32=G2, ...). This "spectral index" is used to interpolate spectral type from measured color index.

The average of all 6 interpolated spectral indices was used to estimate the spectral type of each component of the binary star; the standard deviation (σ) gives a rough indication of the uncertainty of its type. The final results from the speckle photometry method are presented in Table 4. Component color indices are compared with APASS10 (unresolved). Average spectral index and the correlated spectral type are then compared with WDS spectral types, which are presumably from spectroscopic catalogs.

Orange in Table 4 indicates that the secondary star was not detected, or too faint for photometry, yielding unusable color indices. APASS10 did not include 17465+2743 AC7BC, so ATLAS RefCat2 Sloan magnitudes, transformed from Gaia(DR2), were used (highlighted in green).

Table 4. Results for Color Indices and Binary Component Spectral Types. Columns: WDS binary name, component and magnitude source, color indices, average spectral index, and resulting spectral type.

Binary	Component	Average Color Index						Spectral Index		Estimated Spectral Type	
		(i'-z')	(r'-i')	(g'-r')	(r'-z')	(g'-i')	(g'-z')	Average	σ	Spec Phot	WDS
01024+0504 HDS135AB	A	0.045	0.282	1.573	0.327	1.854	1.900	44.1	7.0	K4.1V	K2
	B	0.198	0.578	2.169	0.776	2.747	2.945	50.0	3.7	M0.0V	K8
	APASS (A+B)	0.075	0.329	1.640	0.404	1.969	2.044	46.1	4.9	K6.1V	
01166+1831 HDS169	A										G5
	B										
	APASS (A+B)	0.260	0.091	0.358	0.351	0.449	0.709	33.1	6.2	G3.1V	
01388-1758 LDS838	A	1.283	1.812		3.095			56.6	1.3	M6.6V	M5.5V
	B	1.334	3.525		4.858			58.3	-	M8.3V	M6V
	APASS (A+B)	1.302	2.179	1.451	3.481	3.630	4.932	55.7	2.7	M5.7V	
17066+0039 BU823	A	0.091	0.141	0.371	0.233	0.513	0.604	34.0	4.7	G4.0V	G5V
	B	0.237	0.305	0.869	0.542	1.175	1.412	44.3	1.1	K4.3V	
	APASS (A+B)	0.134	0.184	0.475	0.318	0.659	0.793	39.2	3.0	G9.2V	
17457+1743 STF2205	A	0.175	0.100	0.773	0.276	0.874	1.049	40.2	5.6	K0.2V	K0
	B	0.231	0.151	0.765	0.383	0.916	1.148	42.1	3.7	K2.1V	
	APASS (A+B)	0.202	0.123	0.769	0.325	0.892	1.094	41.1	5.0	K1.1V	
17465+2743 AC7BC	B	0.541	0.982	1.559	1.523	2.541	3.082	52.2	0.1	M2.2V	M3.5V
	C	0.575	1.131	2.277	1.706	3.407	3.983	53.6	1.0	M3.6V	
	ATLAS (A+B)	0.554	1.033	1.711	1.587	2.744	3.298	52.7	0.4	M2.7V	
17506+0714 STT337	A	-0.062	0.108	0.317	0.046	0.425	0.363	26.1	3.6	F6.1V	F2
	B	-0.068	0.087	0.386	0.019	0.473	0.405	26.3	4.2	F6.3V	
	APASS (A+B)	-0.064	0.099	0.347	0.035	0.446	0.382	26.4	3.9	F6.4V	
18320+0647 STT354	A	-0.129	0.115	0.411	-0.015	0.526	0.396	25.6	7.6	F5.6V	F5V
	B	-0.190	0.006	0.602	-0.184	0.609	0.418	24.7	11.9	F4.7V	
	APASS (A+B)	-0.144	0.087	0.459	-0.057	0.546	0.402	25.3	8.4	F5.3V	
19019+1910 STF2437	A	0.307	0.034	0.294	0.341	0.328	0.635	33.4	9.9	G3.4V	G5
	B	0.279	-0.056	0.333	0.223	0.276	0.556	31.4	10.0	G1.4V	
	APASS (A+B)	0.299	0.000	0.309	0.299	0.309	0.608	32.6	10.1	G2.6V	
20290+0710 A610	A	0.247	0.062	0.357	0.309	0.419	0.667	34.4	8.2	G4.4V	G0
	B	0.137	0.028	0.460	0.165	0.488	0.625	32.4	6.4	G2.4V	
	APASS (A+B)	0.212	0.050	0.397	0.262	0.447	0.659	34.0	7.4	G4.0V	
20329+1142 J1AB	A	0.144	0.154	0.854	0.298	1.008	1.152	41.6	3.1	K1.6V	Unknown
	B	0.222	0.316	1.077	0.538	1.393	1.615	45.1	0.8	K5.1V	
	APASS (A+B)	0.173	0.210	0.922	0.383	1.132	1.305	43.3	1.2	K3.3V	
20329+1357 L35CD	C	0.142	0.282	0.919	0.424	1.201	1.343	43.6	0.2	K3.6V	K0
	D	0.039	0.190	0.767	0.229	0.957	0.996	39.3	4.4	G9.3V	
	APASS (A+B)	0.119	0.249	0.854	0.368	1.103	1.222	43.1	0.4	K3.1V	
20524+2008 HO144	A	0.346	0.222	0.629	0.568	0.851	1.197	43.8	3.4	K3.8 (III?)	F7III (F5)
	B	0.418	-0.404	-0.061	0.014	-0.465	-0.048	20.0	17.0	F0.0V	A7V (A0)
	APASS (A+B)	0.360	0.079	0.386	0.439	0.465	0.825	36.6	9.2	G6.6V	
21186+1134 BU163	A	-0.085	0.086	0.937	0.001	1.022	0.937	32.7	11.6	G2.7V	G0V
	B	0.000	0.035	1.109	0.035	1.144	1.144	34.6	10.5	G4.6V	G6V
	APASS (A+B)	-0.070	0.077	0.965	0.007	1.042	0.972	33.0	11.5	G3.0V	
22419+2126 STF2934	A	-0.118	0.155	0.423	0.036	0.578	0.460	27.7	8.0	F7.7V	G0
	B	-0.151	0.235	0.597	0.084	0.832	0.681	32.6	12.4	G2.6V	
	APASS (A+B)	-0.128	0.178	0.470	0.050	0.648	0.520	29.4	9.9	F9.4V	
22557+1547 HU987	A	0.180	0.127	0.156	0.306	0.283	0.462	32.3	9.2	G2.3V	G5
	B	0.320	0.169	0.306	0.493	0.475	0.796	37.7	8.4	G7.7V	
	APASS (A+B)	0.233	0.142	0.205	0.375	0.347	0.580	33.9	9.0	G3.9V	
23024+1837 HU398	A		0.161	0.591		0.753		38.7	1.5	G8.7V	G5
	B		0.122	0.566		0.688		36.1	4.4	G6.1V	
	APASS (A+B)		0.147	0.582		0.729		37.5	3.1	G7.5V	
23409+2022 HO303AB	A		0.352	1.260	0.282	1.612	1.542	44.7	2.8	K4.7V	K2
	B		0.903	1.660	0.951	2.563	2.611	51.3	1.5	M1.3V	
	APASS (A+B)		0.440	1.303	0.394	1.743	1.697	46.1	2.1	K6.1V	

11. Discussion

Following up on the initial validation work from paper I, more binaries were observed, with a larger telescope, under better photometric sky conditions, and generally better results were achieved. These observations revisit, support and confirm most of the findings from paper I.

The results in Tables 3 and 4 are encouraging. Good astrometry and reasonable photometry were achieved in all cases except where the secondary star was not detected in some filters, or the SNR was too low. Faint red secondary stars, when observed in the g′ (blue/green) filter, were particularly challenging, and will require a larger number of speckle frames to boost SNR.

The estimated component spectral types based on average color indices agree quite well with WDS Catalog spectral types. This comparison is shown in Figure 10, where the black line represents perfect agreement. For the three binaries (other than HO144 discussed below) where WDS has spectral types for both components, the Speckle Photometry types are the same within less than 3 sub-types. One binary (J1AB) had no WDS spectral type to compare with, and one other (HDS169) had no successful speckle photometric observations. Of the remaining 12 spectroscopically unresolved binaries (solid symbols), speckle photometry component types straddle the WDS unresolved type

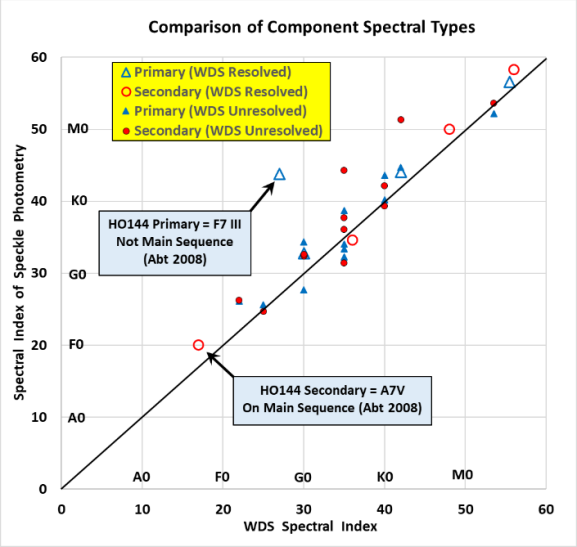

Figure 10. Speckle photometry results for the binary components compared with spectroscopic types in WDS, both resolved and unresolved.

in 7 cases, and the primary is shifted by less than four sub-types in the other 5 cases.

For a few systems in Table 4, the primary star is estimated to have a slightly *later* (i.e., redder) spectral type than the secondary star. This would imply that one or both stars are not on the main sequence. However, in all cases but one, applying the spectral index uncertainties could switch their early/late spectral type relationship. Therefore, all but one of the systems observed are probably main sequence pairs.

The one exception is 20524+2008 HO144 (HD 198810 & HD 198811), which has been resolved spectroscopically and studied by famous astronomers. The WDS types F5+A0, noted in parentheses in Table 4, are from the historic HD catalog extension by Cannon & Pickering (1923). The most recent spectroscopic observation was by Helmut Abt using the Kitt Peak 2.1-meter telescope at higher resolution, who found the spectra to be F7III+A7V (Abt, 2008). This confirms that the secondary star is on the main sequence, but the primary is a giant; the author would not have observed it if that had been known beforehand.

The HO144 speckle photometry results confirm that the primary is much redder than the secondary. However, the primary spectral type is also *significantly later* than Abt's spectroscopic type, as noted in Figure 10. The spread of photometric types between the two components is more than two letter types, while the spectroscopic types are only one letter apart.

The APASS10 unresolved type is shifted to G6.6, about one full letter type beyond the giant (F7III), but the reason for that shift is not known. The speckle photometry types still straddle the APASS10 type as they must. It is likely that the giant primary is incorrectly typed by the speckle photometry method because the Mamajek tables are valid only for the main sequence.

Care must be taken when measuring stacked long exposures to make the aperture large enough to include practically all the light for all filters, so that small percentages of un-measured light will not cause errors among the color indices. However, larger photometric apertures also increase the contribution of background noise.

A practical assumption of the speckle photometry method is to apply the photometric calibration factor derived from *combined* light of both components also to the A and B binary components *individually*. This assumption seems to work well; however, it may introduce systematic errors from 2nd-order extinction, especially for blue/red binary components.

The effects of variable extinction were mostly avoided by observing only on good nights at a fairly good site, but confirmation by actual extinction measurements was not done. It is noted that the photometric approximations used so far – long exposures compared with a source of Sloan secondary standard magnitudes such as APASS10 – might be avoidable through conventional "all-sky"

photometry. At a good site, conventional photometric transformation observations could be made occasionally. Then if nightly extinction coefficients were measured for each filter, there is no reason that rigorous photometric corrections could not be *applied to the instrumental Bispectrum images directly*. As a further development of speckle photometry, the practicality of applying conventional all-sky photometric techniques directly to Bispectrum images should be studied.

All-sky photometry would eliminate any color index errors that may appear in the survey catalog magnitudes, thereby improving the quality of component color indices and spectral types. Only speckle exposures would be required – no "long" exposures – so efficiency of observations and data reduction would also improve. However, uncertainty of measured extinction and transformation corrections would then become a new (but hopefully small) error source. Such observations may be attempted in the future.

12. Conclusions

It has been confirmed that Speckle Tool Box Bispectrum Analysis produces diffraction-limited resolution and correct, repeatable flux distribution between the resolved components of binaries, even for high Δmagnitude pairs.

Repeatability of Flux Proportions is good when primary SNR>50 but may be poor for SNR<50.

Color indices were measured accurately enough to make reasonable estimates of component color indices and corresponding spectral types.

The correlations of spectral type with Johnson-Cousins color indices in the Mamajek tables still produced reasonable spectral types after transformation to the Sloan photometric system.

APASS10 has the most suitable Sloan magnitudes for brighter stars accessible to small telescopes.

Sloan photometry from the AAVSO APASS10 survey provided consistent secondary standard star magnitudes that were used for approximate self-calibration of the unresolved binary. For a few star/filter combinations, a limited number of survey exposures were available, possibly reducing its photometric accuracy.

Use of the simple approximate global calibration factor as a means of self-calibration, does a reasonable job of transforming instrumental magnitudes to standard Sloan magnitudes.

Measuring stacked long exposures requires an aperture large enough to include practically all the light, so that small percentages of un-measured light cannot cause errors among filters and color indices.

Improved consistency of color indices and quality of spectral types may be achievable at photometric sites by careful "all-sky" calibration with true photometric standard stars, and by applying those photometric corrections directly to the Bispectrum flux data.

It is hoped that the speckle photometry method will provide information useful to improve the quality of stellar masses in binary orbit solutions and a more complete picture of stellar properties.

13. Acknowledgements

This research has made use of the Washington Double Star Catalog and 6th Orbit Catalog, maintained at the U.S. Naval Observatory. It has also made use of the APASS database, located at the AAVSO web site. Funding for APASS has been provided by the Robert Martin Ayers Sciences Fund and NSF AST-1412587. This research utilized the SIMBAD, VizieR and Aladin features of the Strasbourg Astronomical Data Center (CDS) and results from the European Space Agency's Gaia mission. Gaia DR2 data was processed by the Gaia Data Processing and Analysis Consortium (DPAC), funded by national institutions participating in the Gaia Multi-Lateral Agreement (MLA).

The author is indebted to Dave Rowe and PlaneWave Instruments for the many outstanding software tools that make speckle data processing easily accessible to amateurs and students, to Dan Gray for his ZWOCam speckle camera control software and patient helpfulness, and to Russ Genet for reviewing this paper, his useful comments, and many years of collaboration. The author very much appreciates use of the 22-inch Kuhn observatory owned and maintained by the Orange County Astronomers. All of these contributions made this work possible.

14. References

AAVSO web site, 2020. https://www.aavso.org/download-apass-data

Abt, Helmut A., 2008. "Visual Multiples IX. MK Spectral Types," *ApJS*, **176**, 216, May 2008.

Cannon, A. J. and Pickering E. C., 1923. "The Henry Draper catalogue: 19h and 20h," *Annals of Astronomical Observations, Harvard College Observatory*, **98**, 0-258, 1923.

Caputo, R., Marchetti, C., Teagarden, J., Armstrong, J.D., Wiese, C., Tock, K., Genet, R., Harshaw, R., Wasson, R., Freed, R., "First Remote Student Speckle Interferometry Double Star Observations on the InStAR Student Robotic Telescope Network," *JDSO*, **16-5**, 458, November 2020.

Carrasco, Josep M., Gaia web site, Section 5.3.7 "Photometric Relationships with Other Photometric Systems," https://gea.esac.esa.int, taken from S. Alam, F. D. Albareti, C. Allende Prieto, F. Anders, S. F. Anderson, T. Anderton, B. H. Andrews, E. Armengaud, É. Aubourg, S. Bailey and et al., 2015. "The 11th and 12th Data Releases of the Sloan Digital Sky Survey: Final Data from SDSS-III." *ApJS,* **219**, pp. 12.

Davidson, James W. Jr., Brian J. Baptista, Elliott P. Horch, Otto Franz, and William F. van Altena, 2009. "A Photometric Analysis of Seventeen Binary Stars Using Speckle Imaging," *The Astronomical Journal*, **138,** pp 1354–1364, November 2009.

Gray, Dan, 2020. Personal communications.

Harshaw, R., Rowe, D., Genet, R., 2017. "The Speckle Toolbox: A Powerful Data Reduction Tool for CCD Astrometry," *Journal of Double Star Observations*, **13-1**, 52, January 2017.

Horch, Elliott P., Zoran Ninkov, Otto G. Franz, 2001. "CCD Speckle Observations of Binary Stars from the Southern Hemisphere – III. Differential Photometry," *The Astronomical Journal*, **121**: 1583, March 2001.

Horch, Elliott P., Meyer, Reed D., van Altena, William F., 2004. "Speckle Observations of Binary Stars with the WIYN Telescope – IV. Differential Photometry," *The Astronomical Journal*, **127**, 1727–1735, March 2004.

Horch, Elliott P., 2006. "The Status of Speckle Imaging in Binary Star Research," *RevMexAA (Serie de Conferencias)*, **25**, 79–82, 2006.

Johnson, H.L. and Morgan W.W., 1953. "Fundamental Stellar Photometry for Standards of Spectral Type on the Revised System of the Yerkes Spectral Atlas," *Astrophysical Journal*, **117**, pp 313–352, 1953.

Mamajek, E.E., 2019. University of Rochester web site of Eric Mamajek: http://www.pas.rochester.edu/~emamajek/EEM_dwarf_UBVIJHK_colors_Teff.txt, Version 2019.3.22.

Marchetti, Calla, Ryan Caputo, and Russell Genet, 2020. "The Fairborn Institute Robotic Observatory: First Observations," *JDSO*, **16-5**, 444, November 2020.

McAlister, Harold A., 1985. "High Angular Resolution Measurements of Stellar Properties," *Annual Review of Astronomy & Astrophysics*, **23**, 59-87, 1985.

Pecaut, M.J. & Mamajek, E.E., 2013. "Intrinsic Colors, Temperatures, and Bolometric Corrections of Pre-Main-Sequence Stars," *ApJS*, **208**, 9, Sept 2013.

Rogers, Christopher T., Ron Canterna, J. Allyn Smith, Michael J. Pierce, and Douglas L. Tucker, 2006. "Improved u' g' r' i' z' to U B V Rc Ic Transformation Equations for Main-Sequence Stars," *The Astronomical Journal*, **132**, pp 989-993, September 2006.

Rowe, D., and Genet, R., 2015. "User's Guide to PS3 Speckle Interferometry Reduction Program," *Journal of Double Star Observations*, **11-1S**, 266, September 2015.

Rowe, D., 2017. "Guide to Using WDS1.2 Search Tool for the WDS Catalog," private communication, 2017.

Rowe, D., 2018. "Guide to GDS1.00 Gaia DR2 Double Star Catalog," private communication, July 17, 2018.

Rowe, D., 2020. "Speckle ToolBox 1.14 Data Reduction Tools," private communication presentation to Stanford On-Line High School students, June 26, 2020.

Tonry, J. L., L. Denneau, H. Flewelling, A. N. Heinze1, C. A. Onken, S. J. Smartt, B. Stalder, H. J. Weiland, C. Wolf, 2018. "The ATLAS All-Sky Stellar Reference Catalog," *The Astrophysical Journal*, **867**, 105, November 10, 2018.

Wasson, R., 2018. "Speckle Interferometry with the OCA Kuhn 22" Telescope," *Journal of Double Star Observations*, **14-2**, 223-241, April 2018.

Wasson, R., 2019. "Speckle Interferometry with the OCA Kuhn 22-in Telescope – II," *JDSO*, **15-2**, 273, April 2019.

Wasson, R., Genet, R., Rowe, D., 2021. "Speckle Photometry and Spectral Types of Close Binary Star Components," *Proceedings for the 40th Annual Symposium of the Society for Astronomical Sciences,* June 2021, 125-145.

Wasson, R., Genet, R., Rowe, D., 2022. "Speckle Photometry and Spectral Types of Close Binary Star Components," *JDSO*, **18-1**, 8, Feb 2022.